On the Role of Desolvation upon the Sodiation of Hard Carbon in Sodium-ion Batteries: A Microcalorimetric Study of the Sodiation Entropy

AUTHOR NAMES

Laurin Derr [a,], Marcel Lang [a], Krishnaveni Palanisamy [b], Christine Kranz [b], Rolf Schuster [a,]**

AUTHOR ADDRESS

[a] Institute of Physical Chemistry, Karlsruhe Institute of Technology, 76131 Karlsruhe, Germany.

[b] Institute of Analytical and Bioanalytical Chemistry, Ulm University, 89081 Ulm, Germany.

AUTHOR INFORMATION

Corresponding Authors

* E-mail: rolf.schuster@kit.edu; laurin.derr@kit.edu

ABSTRACT

Hard carbon (HC) is one of the most promising anode materials for sodium-ion batteries, but the different sodiation processes contributing to its reversible capacity are still under debate. In order to obtain thermodynamic information, we measured the heat exchanged at a single HC composite electrode during the (de-)sodiation of HC in $NaClO_4$/propylene carbonate and $NaPF_6$/Diglyme to determine the reaction entropy of the sodiation process of HC at different states of charge (SoCs). We found that it is dominated by the positive entropy contribution of the concomitant desolvation, leading to reaction entropies up to 85 J mol^{-1} K^{-1} for $NaClO_4$/propylene carbonate and 250 J mol^{-1} K^{-1} for $NaPF_6$/Diglyme, respectively. Together with information of the electrochemical analysis of millisecond charging/discharging pulses we postulate a capacitive adsorption process with incomplete desolvation at low SoC while at medium to high SoC, a Faradaic insertion process with complete desolvation takes place.

INTRODUCTION

Sodium-ion batteries (SIBs) may potentially substitute Lithium-ion batteries (LIBs), especially for applications like stationary energy storage or low-cost vehicles.[1] Reasons are the broad abundance of sodium and its low standard electrode potential close to that of Lithium.[2] While the general working principle of LIBs can be adapted to SIBs, different cathode active materials have to be used, due to the larger ionic radius of Na^+.[2] Also graphite, which is typically used as anode active material, has to be replaced, since Na intercalation into graphite is thermodynamically unfavorable.[3] Meanwhile several cathode and anode material classes were identified and, e.g., the combination of $Na_3V_2(PO_4)_3$/C as cathode active material with hard carbon (HC), the most used anode active material for SIBs,[4] delivered a decent capacity and good cycling stability.[5] However the underlying charge storage mechanism of Na in HC is still under debate.[4,6–9] Thus, this study focuses on HC and its sodiation mechanism.

HC is non-graphitizable carbon consisting of pseudo-graphitic domains, defects and micro- and nanopores and can be derived by pyrolysis from biomass or polymers.[6] Its voltage profile during sodiation generally separates into a sloping region, where the potential is steadily decreasing from 2 V (vs. Na^+/Na) to around 0.1 V and a plateau region below 0.1 V, where the potential only slowly varies with the state of charge (SoC) (see, e.g., Figure 2). First explanations for this behavior were presented by Stevens and Dahn, using wide and small angle X-ray scattering measurements. Based on their experimental data, they postulated that upon charging first the interlayers of the pseudo-graphitic domains and subsequently the pores are filled with sodium,[10] which was denoted as ’intercalation-filling‘ model. The insertion process was intensively studied by various methods, such as, e.g., solid-state NMR,[11–13] electrochemical impedance spectroscopy (EIS),[14–16] Raman scattering,[14,17–19] dilatometry[20,21] or various X-ray scattering methods.[11,12,19,22,23] These

investigations led to several variations of the proposed sodiation mechanism, e.g., the ’adsorption-intercalation-filling‘ model, where adsorption of Na^+ at defects and heteroatoms at higher potentials is followed by intercalation of Na^+ in the graphitic domains at intermediate SoC. Finally, filling of the pores with quasi-metallic Na takes place at low potentials. Alternatively, there are the ’adsorption-filling‘ or the ’adsorption-intercalation‘ models, where the adsorption of Na^+ at high potentials is followed by either filling of the pores with Na or intercalation of Na^+ into the graphitic domains at low potential.[6]

Thermodynamic information on the ongoing electrochemical processes may help to further elucidate the storage mechanism of sodium in HC.[24] One important quantity to describe the thermodynamics of electrochemical processes is the reaction entropy. The potential dependent reaction entropy of a full cell can for example be obtained by measuring the temperature coefficient of the equilibrium cell potential as a function of the SoC. With this so-called entropy profiling, Mercer et al. determined the reaction entropy of a HC/Na-metal cell at different SoCs and explained their results by a transition from Na filling the interlayers to Na filling the nanopores with increasing SoC.[25,26] Since this method is based on the measurement of the equilibrium cell potential, it is very sensitive to small deviations of the cell system from the thermodynamic equilibrium. Particularly at low SoC, where the cell potential is strongly varying during ongoing sodiation, it might be challenging to determine exact values for the temperature coefficient of the cell potential, due to slow equilibration.

To overcome these difficulties we determine the reaction entropy of the processes taking place at the working electrode (WE) by single electrode microcalorimetry.[27,28] By using thin film spray-coated electrodes,[29] the heat generated by the electrochemical reaction is quickly transferred to the electrode’s backside, where a sensitive temperature sensor is mounted. From the temperature

variation of the electrode, the heat that was consumed/produced during the electrochemical reaction, is inferred. Since we apply only short, small current pulses, heat evolution is to a large part reversible. By applying positive and negative current pulses we can precisely determine the reversibly exchanged heat, which gives direct access to the reaction entropy of the processes at the HC composite electrode.[30] In this study, we compare the sodiation of HC in typical SIB carbonate electrolytes, 1 M $NaClO_4$ in propylene carbonate (PC) with and without the additive fluoroethylene carbonate (FEC), and an ether-based electrolyte, 1 M $NaPF_6$ in 1-methoxy-2-(2-methoxyethoxy) ethane (Diglyme), by determining its reaction entropy at different SoCs. Additionally, the response of the electrode potential to millisecond (ms) charging pulses is analyzed to distinguish between the dominating sodiation processes.

EXPERIMENTAL

The HC composite electrodes were fabricated by spray-coating, which is described in detail in Ref.[29]. The water-based slurry consisted of 85 % hard carbon (Kuranode, 5 µm (type II), Kurary, Japan) active material, 5 % sodium carboxymethyl cellulose (CMC, molecular weight ~124000, Sigma Aldrich, Germany) as binder and 10 % carbon black (Vulcan XC72R, Cabot Corporation, USA) as conductive carbon. Using a spray gun, mask spots with 5 mm diameter were spray-coated onto a 50 µm thick Cu foil (99.995 %, Advent). The electrodes were dried overnight at RT and afterwards dried under vacuum at 80 °C. 9 mm electrodes with 5 mm diameter coating in the center were punched out and dried for an additional 2 hours under vacuum at 80 °C, before they were assembled in the electrochemical microcalorimeter cell. The active mass loading was about 1.8 mg cm^{-2} and the coating thickness was 20 µm. As reference and counter electrodes (RE and CE), 1 mm diameter Na wires (99.95 %, Alfa Aesar) were freshly prepared by extrusion form a glass syringe.[31]

The carbonate electrolyte was prepared as described in Ref.[29] by mixing $NaClO_4$ (Alfa Aesar, Germany) with anhydrous propylene carbonate (Sigma Aldrich, Germany). Fluoroethylene carbonate (FEC) (Sigma Aldrich, Germany) was added when required. For the ether-based electrolyte $NaPF_6$ (99+ %, Alfa Aesar) was mixed with Diglyme (99.5 %, Sigma Aldrich). The salt was dried under vacuum at 100 °C for at least 24 h before desolving it in Diglyme.

The used single electrode microcalorimeter is a home-built setup, which was described and schematically shown, e.g., in Ref.[28]. The modifications to the setup, which are needed to enable experiments with non-aqueous electrolytes, were described in Ref.[31]. A description of the experimental procedure with focus on the calibration of the microcalorimeter is given in the Supporting Information.

RESULTS AND DISCUSSION

To ensure reversible and reproducible behavior and a stable solid electrolyte interphase (SEI) on the HC composite electrode during the microcalorimetric pulse experiments, the HC composite electrode was galvanostatically cycled 7 times between 0.005 V and 2 V prior to the experiment. For more details about the electrochemical cycling the reader is referred to the Supporting Information. Then, during the 8^{th} cycle, the charging/discharging was subsequently interrupted at different SoCs and the microcalorimetric pulse experiments were conducted. In Figure 1, the current, potential, temperature and heat transients for a 10 ms long (a) sodiation and (b) desodiation current pulse with a nearly fully sodiated HC (SoC = 93 %, OCP = 46 mV) in $NaClO_4$/PC are shown exemplary for the microcalorimetric pulse experiments. Before and after the current pulse, the cell was set to OCP, meaning that current flow in the outer cell circuit was allowed only during the 10 ms pulse. The current pulse amplitudes in Figure 1 (black lines) correspond to a

charging/discharging rate of 3 C and the SoC changed by about 10^{-5} of the full capacity by a single current pulse. The potential (Figure 1, blue lines) de-/increased stepwise when the current was switched on, followed by a more gradual variation during the 10 ms pulse duration. Reversed behavior is found after switching off the current. The potential relaxes towards its initial potential in about 30 ms. We attribute the instantaneous potential jumps to IR drop caused in the electrolyte during the current flow, while the gradual change may point to concentration overpotential due to depletion or enrichment of Na^+ or Na, in the electrolyte or the HC grains, respectively. A detailed SoC-dependent analysis of the potential response to the short charging/discharging pulses is given below. The temperature signal (Figure 1, red lines) shows cooling during sodiation of the HC composite electrode and heating during desodiation. The temperature reached a minimum/maximum 15 to 20 ms after the end of the current pulse and then relaxed towards the starting temperature, due to heat dissipation into the surrounding. The almost quantitative reversal of the temperature response upon switching between charging and discharging proves that the sodiation/desodiation of HC with short current pulses is a highly reversible reaction.

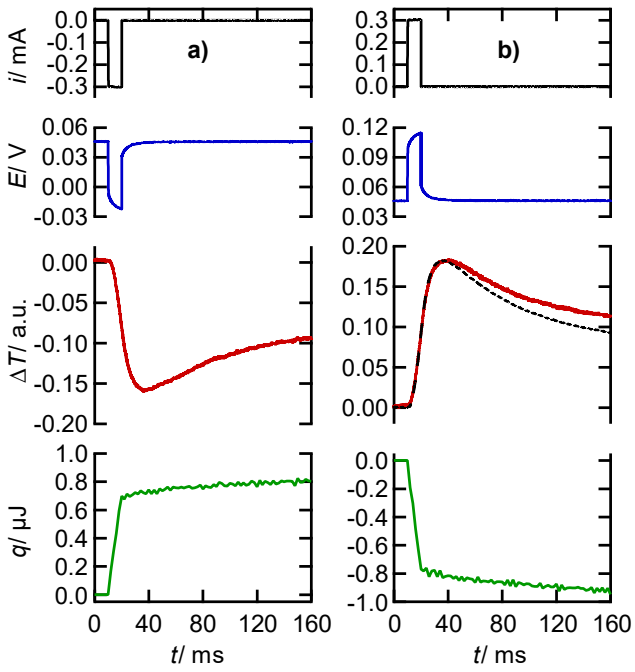

Figure 1. Current i, potential E, temperature ΔT and heat q transients resulting from 10 ms (a) sodiation and (b) desodiation pulses of HC with a charging rate of 3C in $NaClO_4$/PC. The equilibrium potential before the pulse was 46 mV and the SoC of the HC was 93 %. The thermal response to 10 ms blue laser irradiation of the WE (total absorbed energy ca. 3 µJ; for details see SI) is shown in (b) with an adjusted amplitude (black dashed line).

For further interpretation of the temperature transients in Figure 1, we have also included the thermal response of the cell to pulsed 10 ms long laser irradiation of the WE in the same experimental setup. It is shown as the black dashed line (temperature amplitude scaled to fit the maximum of the HC data). For laser heat input, the temperature relaxed faster after its maximum. This indicates that after the sodiation/desodiation pulse, at $t > 20$ ms, cold/heat still evolved without external current flow. This effect can be seen quantitatively in the heat signal (Figure 1, green lines), which was reconstructed from the measured temperature signals employing the thermal response function of the calorimeter as described in detail elsewhere.[32] The absolute value

of the heat was obtained by an *in situ* calibration procedure after the sodiation/desodiation experiment utilizing sodium plating at the electrode, for which the reversibly exchanged heat is known from the literature (for details see SI).[31] It can be seen that most of the heat was exchanged during the current pulse, but considerable heat exchange took place after the pulse (ca. 15 %). We attribute this delayed cold/heat generation, in the absence of current flow in the outer cell circuit, to sodiation/desodiation processes driven by discharging of the interface capacitance during equilibration of the electrode system.[32] Indeed from the potential transients in Figure 1 considerable potential relaxation was observed after the current pulses.

To determine the reaction entropy of the sodiation process from the measured heat transients, irreversible heat contributions due to overpotential had to be accounted for. This was achieved by measuring several sodiation/desodiation pulses with different pulse amplitudes and thus varying contributions from irreversibly exchanged heat. As described in detail in Ref.[33] and in the Supporting Information, interpolation of the molar heat values, which were measured at time t for different overpotentials, to zero overpotential yielded the reversibly exchanged molar heat $q_{\mathrm{m,rev}}(t)$ at time t. This procedure was repeated with the heat measured at times between $t = 0$ ms to $t = 500$ ms with a time interval of 2 ms. In Figure S2, $q_{\mathrm{m,rev}}(t)$ is shown for the nearly fully sodiated HC. The reversibly exchanged heat approaches a steady value at about $t = 400$ ms. Around 85 % of the reversibly exchanged heat, measured at $t = 400$ ms, was already exchanged during the current pulse, up to $t = 20$ ms. Since thermal drift is progressively disturbing the heat values with increasing t, and since we found no significant heat exchange for $t > 400$ ms, $q_{\mathrm{m,rev}}(400\ \mathrm{ms})$ is used in the following as the total reversibly exchanged heat $q_{\mathrm{m,rev}}$ of the sodiation process.

As mentioned before, from the reversibly exchanged heat at the HC composite electrode, usually called Peltier heat, the reaction entropy of the sodiation process can be determined. Since the Peltier heat refers to a single electrode, the transport of electrons and ions across the border of the half-cell during the reaction has to be considered and the reaction entropy of the half-cell reaction is given by $\Delta_R S = q_{\mathrm{m,rev}}/T + \Delta_T S$.[27,30,34] T gives the temperature (298 K) and $\Delta_T S$ corrects for the transport processes. The latter contribution can be approximated[30] and was estimated for 1 M $NaClO_4$ in PC to be -1 J $mol^{-1}K^{-1}$ (and -18 J $mol^{-1}K^{-1}$ for 1 M $NaPF_6$ in Diglyme, respectively).[31] Thus, for the example shown in Figure 1 (SoC 93%), a Peltier heat of 25.8 kJ mol^{-1} yielded a reaction entropy of 86 J $mol^{-1}K^{-1}$ for the sodiation of HC at a SoC of 93 %.

We measured the total reaction entropy for the sodiation process at HC at different SoCs over a complete charging/discharging cycle. The corresponding results for HC in $NaClO_4$/PC are shown in Figure 2 together with the OCP. The error bars of $\Delta_R S$ reflect the relative errors of the data points of one experimental series. They were obtained from the standard deviations of the linear fits during the determination of the reversibly exchanged molar heat (see Supporting Information for further details). The absolute errors from reproducibility and uncertainties of the calibration amount to about 10 % of the reaction entropy. With increasing SoC, a steep increase of the reaction entropy at SoCs below 40 mAh g^{-1} is followed by a broad maximum. Upon discharging, the reversed behavior is found. The broad maximum ranges between 80 and 90 J $mol^{-1}K^{-1}$, which is around the reaction entropy for sodium bulk deposition from the same electrolyte of 83 J $mol^{-1}K^{-1}$ measured in Ref.[31] (black dashed line in Figure 2). Supplementary experiments where 2 wt.% FEC was added to the electrolyte showed that the additive only insignificantly influenced the obtained reaction entropy (see Figure S7). Thus, the following discussion for the additive free electrolyte can be adapted. The strongly positive entropy change upon sodiation can be explained

with the entropy gain from the release of the solvent shell of the Na^+ ions overcompensating the entropy loss due to their fixation in the HC composite electrode – similar to the behavior already described for Na or Li metal deposition.[31,35] The small variations of the sodiation entropy at high SoC (above 40 mAh g^{-1}) shown in Figure 2, we attribute to small variations (< 10 J $mol^{-1}K^{-1}$) of the configurational entropy of Na inserted into the HC, which obviously stays close to that of metallic Na.

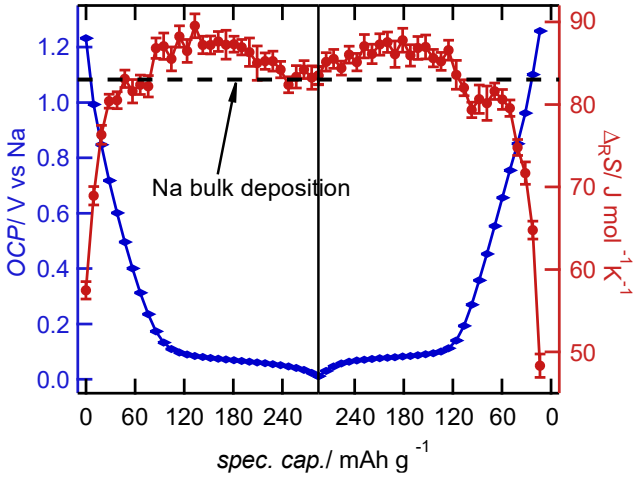

Figure 2. Reaction entropy $\Delta_R S$ (red) and open circuit potential (OCP) (blue) for a complete charging/discharging cycle of HC in $NaClO_4$/PC. The error bars of the reaction entropy indicate the relative errors within a single experimental series (see text). The lower potential limit was 0.005 V and the upper potential limit was 2 V. The vertical black line separates the sodiation and desodiation cycle. For comparison the reaction entropy of Na bulk deposition in $NaClO_4$/PC (83 J $mol^{-1}K^{-1}$) is indicated with the horizontal black dashed line.

Similar variations in the entropy of Na in HC have recently been discussed by Mercer et al.[25] and Wei et al.[36] They employed entropy profiling to measure the reaction entropy of HC/Na metal cells. Since with this approach, the sum of the reaction entropy of both electrodes was measured, for comparison with our data (Figure 3), the reaction entropy of the reference electrode, i.e., Na

metal deposition in $NaClO_4$/PC, was subtracted from our measured reaction entropy. At medium to high SoC (20 to 100 %), the reaction entropies obtained by the different experimental approaches are in good agreement. Mercer et al. explained the entropy variations, with the configurational entropy of a lattice gas model with two energy levels. Within this model, the broad maximum was attributed to a transition of the Na insertion process, from filling of the interlayers of graphitic domains and pores, to sole pore filling. It stands to reason that this interpretation can be adapted to our results. However, at low SoCs (0 to 20 %), Mercer et al. found reaction entropies, which are up to 40 J $mol^{-1}K^{-1}$ higher than the reaction entropy for Na metal bulk deposition. In contrast, we measured reaction entropies, that were significantly lower than that of Na bulk deposition for SoCs below 15 %. These differences might be explained by the different timescales covered by the applied experimental approaches. With microcalorimetry, we evaluate the heat evolved by processes up to 400 ms, whereas entropy profiling monitors equilibration processes on the timescale of several 10 minutes.

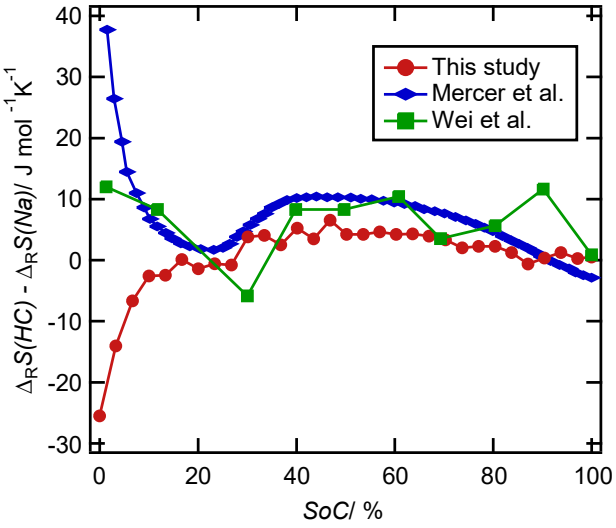

Figure 3. Comparison of the reaction entropy obtained by different studies. The values from this study (red) were shifted by the reaction entropy of Na metal deposition to be comparable with the

entropy profiling studies by Mercer et al.[25] (blue) and Wei et al.[36] (green), who measured the reaction entropy of complete HC/Na metal cells. Data from Mercer et al. reproduced with permission from Ref.[25], Copyright 2022, John Wiley and Sons. Data from Wei et al. reproduced with permission from Ref.[36], Copyright 2022, IOP Publishing.

This implies that at low SoC the charging process may be composed of reaction steps on different time scales. A first clue may be inferred from the shape of the potential transients upon short charging pulses. Typical potential responses to 10 ms charging pulses with -2 mA cm^{-2} amplitude at low and high SoC are compared in Figure 4a, referenced to the respective OCP before the pulse. For both SoCs, the IR drop shows up in Figure 4a as positive potential jumps at $t = 10$ ms and negative ones at $t = 20$ ms, with similar magnitudes for both SoCs. However, during current flow (indicated by the grey background) at low SoC (OCP 0.993 V, light blue) the potential increases nearly linearly, whereas at high SoC (OCP 0.047 V, dark blue) the potential only slightly varies during the pulse. This indicates that at low SoC the dominating process during the current pulse is capacitive in nature, while at high SoC mainly Faradaic processes take place without substantial polarization of the interface. Additionally, the potential relaxation at low SoC considerably continues also after $t = 50$ ms, while for high SoC the initial potential is essentially reached within that time span. This is confirmed with the data shown in Figure 4b, where the deviation of the potential at $t = 400$ ms from the OCP before the current pulse is compared for different SoCs. It can be clearly seen that for SoCs below about 30 mAh g^{-1} significant charging of the interface occurs by the current pulses. Note that the equilibration of the interface and discharging of the interfacial capacitance continues far beyond 400 ms for low SoC. This can be inferred from the slope of the OCP curve vs. specific capacity in Figure 2, which was measured with a waiting time of 40 min after changing the SoC. According to that curve, at 3 % SoC, a pulse charge of 0.0031

mAh g^{-1} as applied in the pulse experiments of Figure 4a would result in an OCP variation of only 0.07 mV. In other words, at low SoC below 15 %, the sodiation/desodiation process is composed of a fast electrochemical process on the ms-timescale, followed by a slow equilibration continuing up to minutes or even hours. Similar findings were obtained with EIS by Schutjajew et al.[15] A candidate for the fast electrochemical process at low SoC might be a capacitive adsorption process of sodium at the HC surface. Similar processes have been discussed for the reversible ion adsorption responsible for energy storage in electrochemical double layer capacitors,[37] for which also HC can be used as electrode material.[38] In contrast, at SoCs above 15 %, the fast electrochemical process becomes Faradaic in nature, i.e., after switching off the external current, the electrode potential quickly returns to its value before the charging pulse. For such a process, Li et al. proposed a mechanism similar to metal underpotential deposition by which the pores are filled with Na.[39] Since with our microcalorimetry method, we evaluate heat evolution only up to 400 ms, we measure the reaction entropy of the fast electrochemical processes. As shown in Figure 2, for SoC below 15 %, we found a reaction entropy substantially smaller (by up to 30 J $mol^{-1}K^{-1}$) than for the Faradaic processes at higher SoCs. This can be readily explained by adsorption of only partly desolvated Na^+ at the HC surface. If only part of the solvation shell is released during the adsorption of Na species at HC, less entropy is gained in comparison to metal-like Na deposition with full desolvation.

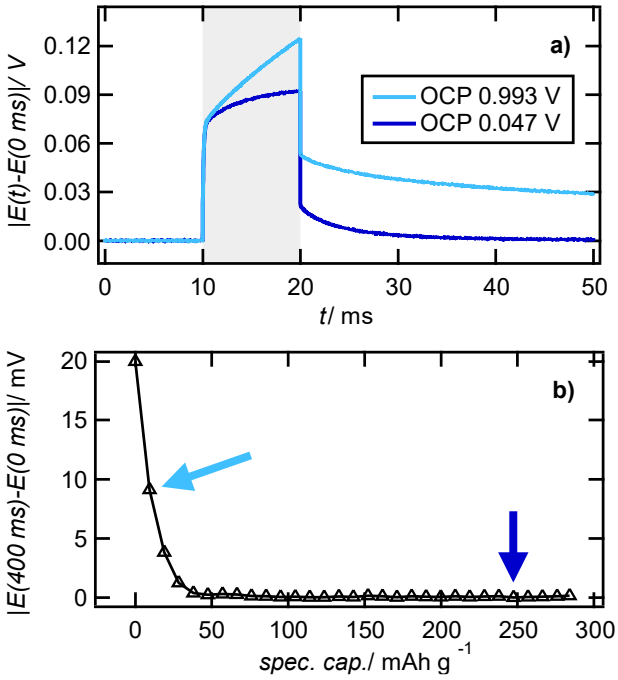

Figure 4. Different details of the microcalorimetric pulse experiments of HC in $NaClO_4$/PC. (a) Potential, referenced to the OCP before the pulse, upon a 10 ms sodiation pulse with a 4C rate (-2 mA cm^{-2}, time interval marked in grey) for two different SoCs. (b) Deviation of the potential at $t = 400$ ms from the OCP before the pulse after a 10 ms sodiation pulse (-2 mA cm^{-2}) for the sodiation cycle dependent on the SoC.

To corroborate our hypothesis that the reduced reaction entropy of sodiation at low SoC can be attributed to adsorption of partially desolvated Na species, we performed experiments in $NaPF_6$/Diglyme as a different electrolyte solution. In this electrolyte, the desolvation entropy of Na^+ was found to be considerably higher than in $NaClO_4$/ PC.[31] We thus expect stronger variations of the reaction entropy with the solvation state. In Figure 5, the SoC-dependent reaction entropies for both electrolytes are shown. The dashed lines indicate the reaction entropies for the Na metal bulk deposition from the respective electrolytes (83 J $mol^{-1}K^{-1}$ for $NaClO_4$/PC and 234 J $mol^{-1}K^{-1}$ for $NaPF_6$/Diglyme[31]). Indeed, the increase in reaction entropy at low SoCs (0 to 20 %) is steeper

and significantly larger for the Diglyme electrolyte. This is compatible with the afore postulated partial desolvation of adsorbed Na^+. Note that our finding may also be in line with co-intercalation of Diglyme and Na in HC. A co-intercalation mechanism in HC was proposed for ether-based electrolytes by several studies utilizing transmission electron microscopy, X-ray diffraction and X-ray photoelectron spectroscopy.[40–42] However, Escher et al.[21] argue against such a solvent co-intercalation mechanism based on the rather small volume expansions found by electrochemical dilatometry. For high SoCs above 20% in both electrolytes, the reaction entropy approximately reaches the respective values for bulk Na deposition, implying complete desolvation. As pointed out before, the small variations around the Na metal deposition entropy can be explained with varying contributions of configurational entropy of adsorbed or deposited Na at the different sites of the HC.

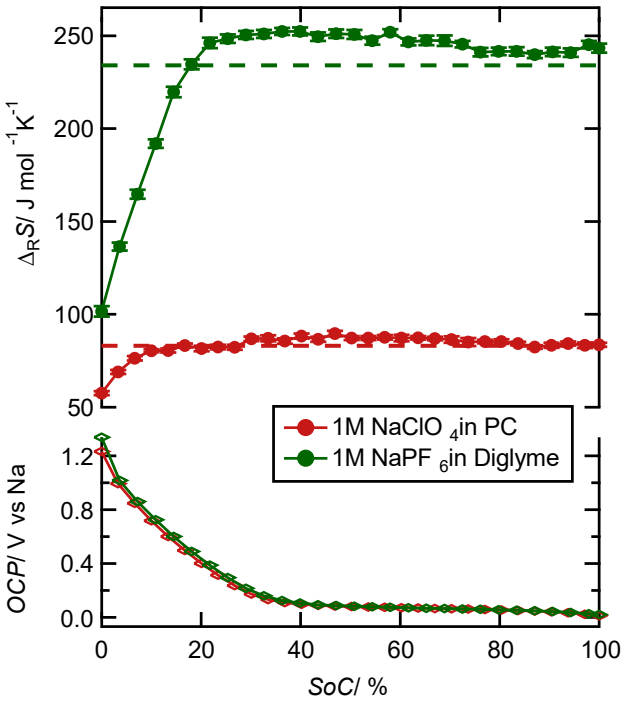

Figure 5. Reaction entropy and OCP for the sodiation cycle of HC in $NaClO_4$/PC (red) compared with $NaPF_6$/Diglyme (green). The error bars of the reaction entropy indicate the relative errors

within a single experimental series (see text). The reaction entropies of the Na bulk deposition from the respective electrolyte are shown with the dashed lines.

CONCLUSIONS

The SoC-dependent reaction entropy of the sodiation of HC in $NaClO_4$/PC and $NaPF_6$/Diglyme was determined by measuring the reversibly exchanged heat at a single HC composite electrode. At high SoC, the entropy change upon desolvation of the Na^+ ions dominates the reaction entropy and the contribution from configurational entropy is rather small, which is consistent with the literature. However, at low SoC, i.e. at potentials exceeding about 0.7 V, we found a fast capacitive adsorption process with rather small entropy changes, pointing to the adsorption of partially desolvated Na^+ ions followed by slow equilibration processes without external current flow. At medium to high SoC This fast capacitive process turns into a fast Faradaic sodiation process with complete desolvation.

ASSOCIATED CONTENT

Supporting Information. Experimental method, determination of time-dependent reversible heat, electrochemical cycling, influence of FEC on the reaction entropy and additional Figures S1-S7.

Data Availability Statement. The data underlying this study are openly available in zenodo at [URL], reference number xxx.

Notes

The authors declare no competing financial interest.

ACKNOWLEDGMENT

We thank Julian Becherer, Stefan Mück and Reiner Mönig for providing the Diglyme electrolyte solution. This work contributes to the research performed at CELEST (Center for Electrochemical Energy Storage Ulm-Karlsruhe) and was funded by the German Research Foundation (DFG) under Project ID 390874152 (POLiS Cluster of Excellence).

REFERENCES

(1) Tapia-Ruiz, N.; Armstrong, A. R.; Alptekin, H.; Amores, M. A.; Au, H.; Barker, J.; Boston, R.; Brant, W. R.; Brittain, J. M.; Chen, Y.; et al. 2021 Roadmap for Sodium-Ion Batteries. *J. Phys. Energy* **2021**, *3* (3), 031503. DOI:10.1088/2515-7655/ac01ef.
(2) Yabuuchi, N.; Kubota, K.; Dahbi, M.; Komaba, S. Research Development on Sodium-Ion Batteries. *Chem. Rev.* **2014**, *114* (23), 11636–11682. DOI:10.1021/cr500192f.
(3) Wang, Z.; Selbach, S. M.; Grande, T. Van Der Waals Density Functional Study of the Energetics of Alkali Metal Intercalation in Graphite. *RSC Adv.* **2013**, *4* (8), 4069–4079. DOI:10.1039/C3RA47187J.
(4) Dou, X.; Hasa, I.; Saurel, D.; Vaalma, C.; Wu, L.; Buchholz, D.; Bresser, D.; Komaba, S.; Passerini, S. Hard Carbons for Sodium-Ion Batteries: Structure, Analysis, Sustainability, and Electrochemistry. *Mater. Today* **2019**, *23*, 87–104. DOI:10.1016/j.mattod.2018.12.040.
(5) Stüble, P.; Müller, C.; Klemens, J.; Scharfer, P.; Schabel, W.; Häringer, M.; Binder, J. R.; Hofmann, A.; Smith, A. Enabling Long-term Cycling Stability of $Na_3V_2(PO_4)_3$/C *vs* . Hard Carbon Full-cells. *Batter. Supercaps* **2023**, e202300375. DOI:10.1002/batt.202300375.
(6) Matei Ghimbeu, C.; Beda, A.; Réty, B.; El Marouazi, H.; Vizintin, A.; Tratnik, B.; Simonin, L.; Michel, J.; Abou-Rjeily, J.; Dominko, R. Review: Insights on Hard Carbon Materials for Sodium-Ion Batteries (SIBs): Synthesis – Properties – Performance Relationships. *Adv. Energy Mater.* **2024**, *14* (19), 2303833. DOI:10.1002/aenm.202303833.
(7) Bommier, C.; Mitlin, D.; Ji, X. Internal Structure – Na Storage Mechanisms – Electrochemical Performance Relations in Carbons. *Prog. Mater. Sci.* **2018**, *97*, 170–203. DOI:10.1016/j.pmatsci.2018.04.006.
(8) Chen, X.; Liu, C.; Fang, Y.; Ai, X.; Zhong, F.; Yang, H.; Cao, Y. Understanding of the Sodium Storage Mechanism in Hard Carbon Anodes. *Carbon Energy* **2022**, *4* (6), 1133–1150. DOI:10.1002/cey2.196.
(9) Xie, F.; Xu, Z.; Guo, Z.; Titirici, M.-M. Hard Carbons for Sodium-Ion Batteries and Beyond. *Prog. Energy* **2020**, *2* (4), 042002. DOI:10.1088/2516-1083/aba5f5.
(10) Stevens, D. A.; Dahn, J. R. The Mechanisms of Lithium and Sodium Insertion in Carbon Materials. *J. Electrochem. Soc.* **2001**, *148* (8), A803. DOI:10.1149/1.1379565.
(11) Stratford, J. M.; Kleppe, A. K.; Keeble, D. S.; Chater, P. A.; Meysami, S. S.; Wright, C. J.; Barker, J.; Titirici, M.-M.; Allan, P. K.; Grey, C. P. Correlating Local Structure and Sodium

Storage in Hard Carbon Anodes: Insights from Pair Distribution Function Analysis and Solid-State NMR. *J. Am. Chem. Soc.* **2021**, *143* (35), 14274–14286. DOI:10.1021/jacs.1c06058.
(12) Au, H.; Alptekin, H.; Jensen, A. C. S.; Olsson, E.; O'Keefe, C. A.; Smith, T.; Crespo-Ribadeneyra, M.; Headen, T. F.; Grey, C. P.; Cai, Q.; et al. A Revised Mechanistic Model for Sodium Insertion in Hard Carbons. *Energy Environ. Sci.* **2020**, *13* (10), 3469–3479. DOI:10.1039/D0EE01363C.
(13) Gotoh, K.; Yamakami, T.; Nishimura, I.; Kometani, H.; Ando, H.; Hashi, K.; Shimizu, T.; Ishida, H. Mechanisms for Overcharging of Carbon Electrodes in Lithium-Ion/Sodium-Ion Batteries Analysed by Operando Solid-State NMR. *J. Mater. Chem. A* **2020**, *8* (29), 14472–14481. DOI:10.1039/D0TA04005C.
(14) Aniskevich, Y.; Yu, J. H.; Kim, J.-Y.; Komaba, S.; Myung, S.-T. Tracking Sodium Cluster Dynamics in Hard Carbon with a Low Specific Surface Area for Sodium-Ion Batteries. *Adv. Energy Mater.* **2024**, *14* (18), 2304300. DOI:10.1002/aenm.202304300.
(15) Schutjajew, K.; Tichter, T.; Schneider, J.; Antonietti, M.; Roth, C.; Oschatz, M. Insights into the Sodiation Mechanism of Hard Carbon-like Materials from Electrochemical Impedance Spectroscopy. *Phys. Chem. Chem. Phys.* **2021**, *23* (19), 11488–11500. DOI:10.1039/D1CP00610J.
(16) Linsenmann, F.; Pritzl, D.; Gasteiger, H. A. Comparing the Lithiation and Sodiation of a Hard Carbon Anode Using In Situ Impedance Spectroscopy. *J. Electrochem. Soc.* **2021**, *168* (1), 010506. DOI:10.1149/1945-7111/abd64e.
(17) Lu, Z.; Yang, H.; Guo, Y.; Lin, H.; Shan, P.; Wu, S.; He, P.; Yang, Y.; Yang, Q.-H.; Zhou, H. Consummating Ion Desolvation in Hard Carbon Anodes for Reversible Sodium Storage. *Nat. Commun.* **2024**, *15* (1), 3497. DOI:10.1038/s41467-024-47522-y.
(18) M. Anji Reddy; M. Helen; Axel Groß; Maximilian Fichtner; Holger Euchner. Insight into Sodium Insertion and the Storage Mechanism in Hard Carbon. *ACS Energy Lett.* **2018**, *3* (12), 2851–2857. DOI:10.1021/acsenergylett.8b01761.
(19) Kitsu Iglesias, L.; Antonio, E. N.; Martinez, T. D.; Zhang, L.; Zhuo, Z.; Weigand, S. J.; Guo, J.; Toney, M. F. Revealing the Sodium Storage Mechanisms in Hard Carbon Pores. *Adv. Energy Mater.* **2023**, *13* (44), 2302171. DOI:10.1002/aenm.202302171.
(20) Alptekin, H.; Au, H.; Jensen, A. C.; Olsson, E.; Goktas, M.; Headen, T. F.; Adelhelm, P.; Cai, Q.; Drew, A. J.; Titirici, M.-M. Sodium Storage Mechanism Investigations through Structural Changes in Hard Carbons. *ACS Appl. Energy Mater.* **2020**, *3* (10), 9918–9927. DOI:10.1021/acsaem.0c01614.
(21) Escher, I.; Ferrero, G. A.; Goktas, M.; Adelhelm, P. In Situ (Operando) Electrochemical Dilatometry as a Method to Distinguish Charge Storage Mechanisms and Metal Plating Processes for Sodium and Lithium Ions in Hard Carbon Battery Electrodes. *Adv. Mater. Interfaces* **2022**, *9* (8), 2100596. DOI:10.1002/admi.202100596.
(22) Cai, C.; Chen, Y.; Hu, P.; Zhu, T.; Li, X.; Yu, Q.; Zhou, L.; Yang, X.; Mai, L. Regulating the Interlayer Spacings of Hard Carbon Nanofibers Enables Enhanced Pore Filling Sodium Storage. *Small* **2022**, *18* (6), 2105303. DOI:10.1002/smll.202105303.
(23) Morikawa, Y.; Nishimura, S.; Hashimoto, R.; Ohnuma, M.; Yamada, A. Mechanism of Sodium Storage in Hard Carbon: An X-Ray Scattering Analysis. *Adv. Energy Mater.* **2020**, *10* (3), 1903176. DOI:10.1002/aenm.201903176.

(24) Tian, Z.; Zhang, Y.; Zhu, J.; Li, Q.; Liu, T.; Antonietti, M. A Reanalysis of the Diverse Sodium Species in Carbon Anodes for Sodium Ion Batteries: A Thermodynamic View. *Adv. Energy Mater.* **2021**, *11* (47), 2102489. DOI:10.1002/aenm.202102489.
(25) M. P. Mercer; S. Affleck; E. M. Gavilán-Arriazu; Zülke, A. A.; P. A. Maughan; S. Trivedi; M. Fichtner; A. R. Munnangi; E. P. M. Leiva; H. E. Hoster. Sodiation Of Hard Carbon: How Separating Enthalpy And Entropy Contributions Can Find Transitions Hidden In The Voltage Profile. *ChemPhysChem* **2022**, *23* (5), 202100748. DOI:10.1002/cphc.202100748.
(26) Mercer, M. P.; Nagarathinam, M.; Gavilán-Arriazu, E. M.; Binjrajka, A.; Panda, S.; Au, H.; Crespo-Ribadeneyra, M.; Titirici, M.-M.; Leiva, E. P. M.; Hoster, H. E. Sodiation Energetics in Pore Size Controlled Hard Carbons Determined via Entropy Profiling. *J. Mater. Chem. A* **2023**, *11* (12), 6543–6555. DOI:10.1039/D2TA09406A.
(27) Schuster, R. Electrochemical Microcalorimetry at Single Electrodes. *Curr. Opin. Electrochem.* **2017**, *1* (1), 88–94. DOI:10.1016/J.COELEC.2017.01.007.
(28) Frittmann, S.; Halka, V.; Jaramillo, C.; Schuster, R. An Improved Sensor for Electrochemical Microcalorimetry, Based on Lithiumtantalate. *Rev. Sci. Instrum.* **2015**, *86* (6), 064102. DOI:10.1063/1.4922859.
(29) Palanisamy, K.; Daboss, S.; Schäfer, D.; Rohnke, M.; Derr, L.; Lang, M.; Schuster, R.; Kranz, C. Spray-Coated Hard Carbon Composite Anodes for Sodium-Ion Insertion. *Batter. Supercaps* **2024**, *7* (1), e202300402. DOI:10.1002/batt.202300402.
(30) Agar, J. N. Thermogalvanic Cells. In *Advances in Electrochemistry and Electrochemical Engineering*; Delahay, P., Ed.; Interscience Publishers: London, 1963; Vol. 3, pp 31–121.
(31) Karcher, F.; Uhl, M.; Geng, T.; Jacob, T.; Schuster, R. Entropic Contributions to Sodium Solvation and Solvent Stabilization upon Electrochemical Sodium Deposition from Diglyme and Propylene Carbonate Electrolytes. *Angew. Chem. Int. Ed.* **2023**, 202301253. DOI:10.1002/anie.202301253.
(32) Bickel, K. R.; Etzel, K. D.; Halka, V.; Schuster, R. Microcalorimetric Determination of Heat Changes Caused by Overpotential upon Electrochemical Ag Bulk Deposition. *Electrochimica Acta* **2013**, *112*, 801–812. DOI:10.1016/J.ELECTACTA.2013.06.056.
(33) Karcher, F.; Uhl, M.; Geng, T.; Jacob, T.; Schuster, R. Detection of Charge-Neutral Near-Equilibrium Processes at Na-Metal Electrodes by Electrochemical Microcalorimetry. *Adv. Energy Mater.* **2023**, 2302241. DOI:10.1002/aenm.202302241.
(34) Ozeki, T.; Ogawa, N.; Aikawa, K.; Watanabe, I.; Ikeda, S. Thermal Analysis of Electrochemical Reactions: Influence of Electrolytes on Peltier Heat for Cu(0)/Cu(II) and Ag(0)/Ag(I) Redox Systems. *J. Electroanal. Chem. Interfacial Electrochem.* **1983**, *145* (1), 53–65. DOI:10.1016/S0022-0728(83)80293-9.
(35) Schmid, M. J.; Bickel, K. R.; Novák, P.; Schuster, R. Microcalorimetric Measurements of the Solvent Contribution to the Entropy Changes upon Electrochemical Lithium Bulk Deposition. *Angew. Chem. Int. Ed.* **2013**, *52* (50), 13233–13237. DOI:10.1002/anie.201305508.
(36) Wei, F.; Li, P.; Zhang, Q.; Shao, G.; Mao, J. Entropy Change Characteristics for Sodium Ion Half/Full Cells Based on Na3V2(PO4)3 and Hard Carbon Materials. *J. Electrochem. Soc.* **2022**, *169* (5), 050503. DOI:10.1149/1945-7111/ac6a14.
(37) Simon, P.; Gogotsi, Y. Materials for Electrochemical Capacitors. *Nat. Mater.* **2008**, *7* (11), 845–854. DOI:10.1038/nmat2297.
(38) Ghosh, S.; Santhosh, R.; Jeniffer, S.; Raghavan, V.; Jacob, G.; Nanaji, K.; Kollu, P.; Jeong, S. K.; Grace, A. N. Natural Biomass Derived Hard Carbon and Activated Carbons as

Electrochemical Supercapacitor Electrodes. *Sci. Rep.* **2019**, *9* (1), 16315. DOI:10.1038/s41598-019-52006-x.
(39) Li, Y.; Vasileiadis, A.; Zhou, Q.; Lu, Y.; Meng, Q.; Li, Y.; Ombrini, P.; Zhao, J.; Chen, Z.; Niu, Y.; et al. Origin of Fast Charging in Hard Carbon Anodes. *Nat. Energy* **2024**, *9* (2), 134–142. DOI:10.1038/s41560-023-01414-5.
(40) Jiang, N.; Chen, L.; Jiang, H.; Hu, Y.; Li, C. Introducing the Solvent Co-Intercalation Mechanism for Hard Carbon with Ultrafast Sodium Storage. *Small* **2022**, *18* (15), 2108092. DOI:10.1002/smll.202108092.
(41) Dong, R.; Zheng, L.; Bai, Y.; Ni, Q.; Li, Y.; Wu, F.; Ren, H.; Wu, C. Elucidating the Mechanism of Fast Na Storage Kinetics in Ether Electrolytes for Hard Carbon Anodes. *Adv. Mater.* **2021**, *33* (36), 2008810. DOI:10.1002/adma.202008810.
(42) Lv, Z.; Li, T.; Hou, X.; Wang, C.; Zhang, H.; Yan, J.; Zheng, Q.; Li, X. Solvation Structure and Solid Electrolyte Interface Engineering for Excellent Na+ Storage Performances of Hard Carbon with the Ether-Based Electrolytes. *Chem. Eng. J.* **2022**, *430*, 133143. DOI:10.1016/j.cej.2021.133143.

TOC GRAPHIC

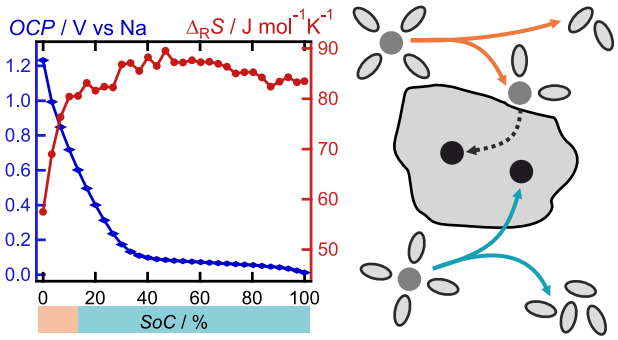
OCP / V vs Na
ΔRS / J mol-1 K-1
1.2
1.0
0.8
0.6
0.4
0.2
0.0
90
80
70
60
50
0
20
40
60
80
100
SoC / %